# **Nanoscale**



PAPER View Article Online
View Journal | View Issue



Cite this: Nanoscale, 2022, 14, 3917

# Assembly mechanism of surface-functionalized nanocubes

Brian Hyun-jong Lee and Gaurav Arya b \*

Faceted nanoparticles can be used as building blocks to assemble nanomaterials with exceptional optical and catalytic properties. Recent studies have shown that surface functionalization of such nanoparticles with organic molecules, polymer chains, or DNA can be used to control the separation distance and orientation of particles within their assemblies. In this study, we computationally investigate the mechanism of assembly of nanocubes grafted with short-chain molecules. Our approach involves computing the interaction free energy landscape of a pair of such nanocubes via Monte Carlo simulations and using the Dijkstra algorithm to determine the minimum free energy pathway connecting key states in the landscape. We find that the assembly pathway of nanocubes is very rugged involving multiple energy barriers and metastable states. Analysis of nanocube configurations along the pathway reveals that the assembly mechanism is dominated by sliding motion of nanocubes relative to each other punctuated by their local dissociation at grafting points involving lineal separation and rolling motions. The height of energy barriers between metastable states depends on factors such as the interaction strength and surface roughness of the nanocubes and the steric repulsion from the grafts. These results imply that the observed assembly configuration of nanocubes depends not only on their globally stable minimum free energy state but also on the assembly pathway leading to this state. The free energy landscapes and assembly pathways presented in this study along with the proposed guidelines for engineering such pathways should be useful to researchers aiming to achieve uniform nanostructures from self-assembly of faceted nanoparticles.

Received 5th December 2021, Accepted 19th February 2022 DOI: 10.1039/d1nr07995f

rsc.li/nanoscale

## Introduction

Self-assembly of faceted nanoparticles (NPs) offers an attractive fabricating approach unique nanostructures. 1-7 In cases where these NPs are made of noble metals, the NP assemblies can exhibit intriguing plasmonic, optical, and catalytic properties that are highly sensitive to the local arrangement of NPs within the structure. 1-3,8-10 Hence, controlling both the translational and rotational order of faceted NPs within their higher-order assemblies is crucial for creating the next generation of nanodevices and materials with desired properties. A simple yet versatile strategy for inducing NPs into specific interparticle distances and orientations involves grafting of ligands such as polymer chains, organic molecules, or DNA onto the NP surfaces. 1-4 While bare NPs, especially those made of materials with large Hamaker constants, tend to assemble into close-packed structures with face-face contacts so as to maximize attractive van der Waals (vdW) interactions between particles, surface functionalization

Department of Mechanical Engineering and Material Science, Duke University, Durham, NC 27708, USA. E-mail: gaurav.arya@duke.edu; Fax: +1 (919) 660-8963; Tel: +1 (919) 660-5435 induces the formation of more open structures with spaced out or slanted faces that reduces the confinement of the grafted ligands between the NP surfaces, leading to lower steric repulsion between the grafts. By modulating this competition between vdW and steric forces through factors such as the length and chemistry of the tethered molecules, the size and material of the NPs, and solvent quality, <sup>1–5</sup> experiments have successfully assembled NP structures with exceptional properties such as plasmonic hotspots <sup>1,11,12</sup> and orientationally disordered crystals. <sup>13,14</sup>

Recently, we investigated the assembly behavior of nanocubes grafted with short-chain molecules. In particular, we used Monte Carlo simulations to compute the free energy landscape of a pair of surface-functionalized nanocubes treated using a coarse-grained model. Analyses of the minimum free energy (MFE) configurations obtained from these landscape revealed that the nanocubes exhibit one of three possible globally stable configurations ("phases"), namely the edge–edge, face–face, and intermediate phases that are distinguished by the amount of grafted ligands they enclose between their apposing faces. Additionally, based on how the MFE configuration varied with certain material parameters, we were able to build a comprehensive phase diagram of nanocube configurations in this parameter space. While the

simulations correctly predicted and explained many of the experimentally observed interparticle configurations in assemblies of polymer-grafted nanocubes, two important aspects of the assembly mechanism were not addressed. First, experiments have demonstrated that nanocubes do not assemble into a single configuration but exhibit multiple different configurations. 1-3 This suggests that not all of the nanocubes may have assembled into their global MFE or stable configuration and that some may have assembled into local MFE or metastable configurations. Second, some experiments have reported that nanocubes which initially assemble into edgeedge configurations transitioned into face-face configurations after they were thermally annealed.1 This implies that, while the face-face configuration was the more energetically favored state, the nanocubes first assembled into a metastable edgeedge state and required higher thermal energy to transition into their globally stable state. Both sets of experimental results suggest that a full understanding of the metastable configurations exhibited by our nanocubes and the mechanism of transition between these states is crucial for controlling the assembled configurations of faceted NPs.

The task of identifying metastable states and determining transition pathways is not trivial, as the configurational free energy landscape of anisotropic NPs, even a pair of them, is multidimensional. This is in sharp contrast to spherical NPs whose pairwise interactions can be fully described by a single coordinate, the separation distance between NPs. This difficulty can be overcome through the minimum free energy pathway (MFEP) analysis commonly employed in biophysics to understand how proteins undergo functionally relevant transitions across metastable and stable states. While a pair of such states can be connected by an infinite number of pathways, there usually exists a unique pathway which minimizes the path-integral of free energy amongst all possible pathways. This pathway, termed the MFEP, represents the most probable pathway taken by the system to transition between the two states. By analyzing the conformational changes and the energetic barriers associated with this pathway, the kinetics and mechanism of the transition between two metastable states or between a metastable and a stable state can be obtained.

In this study, we employ our previously utilized simulation model of surface-functionalized nanocubes<sup>15</sup> and undertake a free energy landscape based MFEP analysis to investigate the assembly mechanism of a pair of such nanocubes. Our results show that the two-particle interaction free energy landscapes are inhabited by multiple metastable states and that transitions between these states along the MFEPs incur large energy barriers, leading to unusually slow transition rates. We find that the incorporation of surface roughness of nanocubes is required to reduce the heights of these barriers and bring the transition rates to within experimental time scales. Analysis of configurations along the MFEPs reveals that the nanocubes transition to their globally stable configurations through association and dissociation steps involving a combination of sliding, rolling, and lineal motions. Importantly, the MFEPs are able to explain the experimentally observed

phenomena of nanocubes exhibiting a distribution of configurational states within assemblies and of thermal annealing inducing transitions from metastable to stable states.

## Computational methods

#### System configuration

The experimental system of interest consists of nanocubes embedded in a thin liquid film, where confinement and interfacial effects cause the NPs to lie flat and parallel to the airliquid interface. 1-3 Thus, in our model, we assume that the nanocubes cannot exhibit translational or rotational motion in the z direction normal to the film surface. To describe the interparticle configuration of two nanocubes constrained to such quasi-2D environment, we consider that one of the nanocubes is at the origin with its facets parallel to the Cartesian axes and use the following three coordinates to describe the position and orientation of the other nanocube (Fig. 1a): the minimum distance of approach  $d_s$  between the surfaces of the nanocubes along the x axis, the lateral offset  $d_y$  of the nanocubes in the y axis, and the relative orientation  $\theta$  of the nanocubes. This coordinate system was chosen as it conveniently represents the mechanism of nanocube assembly (see Fig. 1b). For example, the association and dissociation of the nanocubes through a sliding motion can be completely described by changes in a single variable,  $d_v$ . Similarly, variations in  $d_s$  and  $\theta$  represent lineal (head-on translation) and rolling motions, respectively.

#### Coarse-grained model

To obtain the interaction energy between the nanocubes in a computationally efficient manner, we utilized a simple coarsegrained model of surface-functionalized nanocubes employed in our previous study that captured sufficiently well the geometry and interactions of ligand-grafted nanocubes. 15 Briefly, the nanocubes were treated as rigid bodies carved out of a simple cubic lattice of beads representing groups of atoms, and the grafted ligands were treated using a bead-spring model, where each bead represented a short segment of the ligand. In addition to these nanocubes that we termed ideal nanocubes, we also studied rough nanocubes with a topography consistent with that measured experimentally. 16 These rough nanocubes were modeled by attaching an extra 24% surface beads at random positions on each face of the nanocubes. All beads in the system interact with each other via the Lennard Jones (LJ) potential  $U_{\text{LI}} = 4\varepsilon_{ij} [(\sigma_{ij}/r_{ij})^{12} - (\sigma_{ij}/r_{ij})^{6}]$ , where  $\varepsilon_{ij}$ ,  $\sigma_{ij}$ , and  $r_{ij}$  represent the LJ energy and size parameters and the separation distance of the interacting beads i and j. The intramolecular interactions of the tethered chains were described by harmonic bond stretching and bending potentials  $U_s = \frac{1}{2}k_s(l-l_0)^2$ and  $U_{\rm b} = \frac{1}{2} k_{\rm b} (\theta - \theta_0)^2$ , where  $k_{\rm s}$  and  $k_{\rm b}$  represent force constants, l and  $\theta$  the bond length and angle, and  $l_0$  and  $\theta_0$  their corresponding equilibrium values. The ligands were attached to each nanocube face in a square pattern, also via harmonic springs of parameters  $k_s$  and  $l_0$ . The solvent molecules were

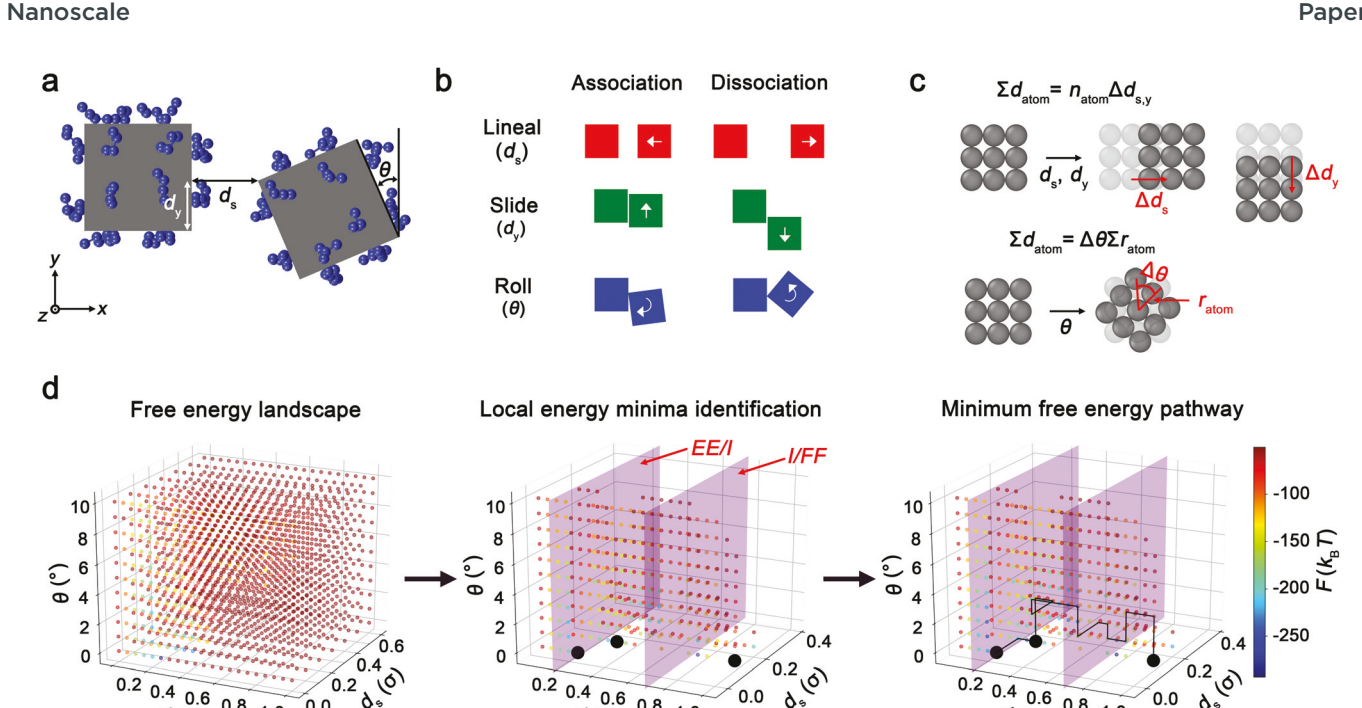


Fig. 1 Schematics of the computational approach. (a) Coarse-grained model of surface-functionalized nanocubes with the coordinate system for describing their interparticle configuration. (b) Mechanism of nanocube association and dissociation involving lineal, sliding, and rolling motions. (c) Definition of the reaction coordinate based on total displacement of nanocube atoms. (d) Procedure for obtaining the MFEP, which involves computation of the free energy landscape, identification of the local energy minima corresponding to the EE, I, and FF phases, and determination of the MFEP by connecting local energy minima via the Dijkstra algorithm. Solid black circles represent the MFE configurations corresponding to the three phases and the purple planes represent boundaries between the three phase domains.

treated implicitly and their effects on the interaction between nanocubes is embedded in the interaction parameters  $\varepsilon_{ii}$  of the ligands and nanocubes. We note that our model accounts only for weak vdW interactions and steric hindrance between ligands and is not suitable for nanocubes grafted with ligands exhibiting strong attractive interactions, such as hydrogen bonding,  $\pi$ – $\pi$  stacking, or electrostatic interactions. Experiments<sup>4,6,17</sup> and simulations<sup>18</sup> on DNA-grafted NPs, where such interactions play a larger role, have shown that they exhibit novel assembly behavior including reconfigurable or chiral nanostructures that cannot be captured by our

Following previous work, 15 the LJ size parameter  $\sigma_{cc}$  for interactions between nanocubes was set equal to  $0.4\sigma$  and the nanocube side length  $D = 10\sigma$ , where  $\sigma$  represents an arbitrary length scale. The LJ energy parameter  $\varepsilon_{cc}$  was varied between 0.25 to  $3\varepsilon$  to probe the role of vdW interactions, where  $\varepsilon$  represents an arbitrary energy scale. Unless indicated otherwise, we fixed the temperature to  $T = \varepsilon/k_{\rm B}$ , where  $k_{\rm B}$  is the Boltzmann constant; thus,  $\varepsilon$  effectively varies between 0.25 to  $3k_{\rm B}T$ . The LJ size parameter  $\sigma_{\rm lig}$  for ligand-ligand interactions was varied between 0.25 to  $1\sigma$  to probe the effects of ligand segment excluded volume, and  $l_0$  and  $\theta_0$  were set equal to  $\sigma_{\text{lig}}$ and 180°. The LJ size parameter  $\sigma_{lc}$  for the interactions between nanocube and ligand beads was obtained using the Lorentz-Berthelot mixing rule:<sup>19</sup>  $\sigma_{lc} = (\sigma_{cc} + \sigma_{lig})/2$ . The LJ energy parameters  $arepsilon_{
m lig}$  and  $arepsilon_{
m lc}$  for ligand-ligand and ligandnanocube interactions were kept fixed at  $0.1\varepsilon$  to model weak interactions mediated by the ligands in good solvent.1-3 To reduce computational cost, we employed a cutoff distance of  $3\sigma$  for LJ interactions between ligands or those between ligands and nanocubes, as these interactions were calculated on the fly at each simulation step due to changing ligand conformations. However, no such cutoff was needed for LJ interactions between nanocube beads, which remained fixed during simulations and were therefore calculated only once before each simulation. The intramolecular force constants  $k_s$ and  $k_b$  were set equal to  $10\varepsilon/\sigma$  and  $0.1\varepsilon/\text{rad}^2$  to describe flexible chains. The length L and grafting density  $\Gamma$  of the ligands were fixed to 4 beads and 0.04 chains per  $\sigma^2$  to model short chains to ensure that the steric repulsion between chains remains weaker than the vdW interactions to allow nanocube assembly. A detailed description of the model is provided elsewhere. 15

#### Minimum free energy pathway

The MFEPs were obtained through the steps illustrated in Fig. 1d. First, we calculated the free energy landscape  $F \equiv F(d_s)$  $d_{\nu}$ ,  $\theta$ ), which is essentially the potential of mean force (PMF) of two nanocubes obtained as a function of their interparticle configuration. To obtain the PMF, we first computed  $f_x$  ( $d_s$ ,  $d_y$ ,  $\theta$ ), the ensemble average of the x-component force acting between the two nanocubes, at all separation distances  $d_s$ within a cutoff distance of  $d_{\text{cut}}$  where the force has decayed to zero. To compute these forces, the nanocubes were held fixed

at each configuration while ligand conformations were sampled using a configurational-bias Monte Carlo method.<sup>20</sup> The forces were then integrated according to  $F(d_s, d_y, \theta) =$  $-\int_{d_{cov}}^{d_s} f_x(\xi, d_y, \theta) d\xi$  to obtain the PMF. The free energy landscape was obtained for the range  $d_s \in (0, 8\sigma)$ ,  $d_v \in (0, 10\sigma)$ , and  $\theta \in (0^{\circ}, 45^{\circ})$  at a resolution of  $0.1\sigma \times 0.4\sigma \times 1^{\circ}$ . We refer readers to our previous study for more detailed explanation of this procedure.15

Next, we located the minima in this free energy landscape corresponding to the phases reported earlier. 15 In particular, we showed that nanocubes can assemble into three types of configurations-face-face (FF), intermediate (I), or edge-edge (EE) states—depending on the amount of ligands enclosed by the interacting faces of the nanocubes. Specifically, the FF, I, and EE states represent nanocubes that confine all, a fraction, or none of the ligands, respectively. In the coordinate system employed in this study (Fig. 1a), these phases are captured well by a single variable,  $d_v$ : configurations with  $d_v \ge 0.75D$  for  $\Gamma = 0.04/\sigma^2$  nanocubes are in the FF state as they lead to all of the grafted ligands being enclosed by the interacting surfaces of the nanocubes; configurations with  $0.75D > d_v \ge 0.25D$ belong to the I state; and those with  $d_v < 0.25D$  are in the EE state as the interacting faces do not confine any ligand. Therefore, to obtain the energetically stable configuration of the nanocubes for each phase, we identified the local free energy minimum within these specified  $d_{\nu}$  bounds corresponding to each of the three phases.

Lastly, the MFEPs between the identified free energy minima were obtained by finding the path of least action<sup>21</sup> connecting the minima. In general, such pathways are obtained either through chain-of-states type of methods, such as nudged elastic band<sup>22,23</sup> or string<sup>24</sup> methods, or algorithms based on graph theory.25-29 For this study, the graph theory approach was used as it is more appropriate for extracting the MFEP from a pre-computed free energy landscape. Specifically, we treat the free-energy landscape as a weighted network in which each configuration is represented as a node that is connected to its adjacent nodes (i.e., configurations at the adjacent grid point in either  $d_s$ ,  $d_v$ , or  $\theta$ ) with weights equal to the differences in their free energies. The MFEPs were then computed by finding the shortest paths between the nodes corresponding to the local MFE configurations through the Dijkstra algorithm implemented in MATLAB. 30,31

#### Reaction coordinate and transition rates

To facilitate analysis of the MFEPs, we defined a reaction coordinate that represents the MFEP as a 1D pathway. In this reaction coordinate, changes in nanocube configuration due to the different modes of displacement  $(d_s, d_v, \text{ or } \theta)$  are equalized in terms of the cumulative distance by which the atoms of the nanocube get displaced via each mode (Fig. 1c). For instance, a  $\Delta d_{\rm s}$  change in separation distance between the nanocubes would lead to a cumulative displacement of  $n_{\rm atom}$   $\Delta d_{\rm s}$ , where  $n_{\text{atom}}$  is the number of atoms in the nanocube. Similarly, rotation of the nanocubes by an angle  $\Delta\theta$  would lead to a cumulative displacement of  $\Delta\theta \sum_{\text{atom}} r_{\text{atom}}$  equal to the sum of the arc lengths travelled by all atoms, where  $r_{\text{atom}}$  is the radial distance of each atom from the nanocube center along the x-y plane. Using this definition, the reaction coordinate which we denote by  $\chi$  is given by the cumulative distance travelled by the nanocube atoms due to changes in nanocube configuration as they progress through the MFEP starting from a suitable initial configuration:

$$\chi \equiv \frac{\sum\limits_{i \in \text{MFEP}} \left( n_{\text{atom}} \left| \Delta d_{s,i} \right| + n_{\text{atom}} \left| \Delta d_{y,i} \right| + \left| \Delta \theta_i \right| \sum\limits_{\text{atom}} r_{\text{atom}} \right)}{n_{\text{atom}} D}. \quad (1)$$

Here, the outer summation runs over the traversed nanocube configurations and the cumulative distance is normalized by  $n_{\text{atom}}D$  so that nanocubes undergoing transition from a tipto-tip to a FF configuration through purely sliding motion would lead to a reaction coordinate value of 1.

The transition rates between the free energy minima in the MFEPs were obtained using Kramers' theory, which provides a closed-form solution to the rate of escape of a thermally equilibrated system over an energy barrier. 32,33 The theory is applicable when the system dynamics are well described by a 1D free energy landscape and the energy barrier is much larger than thermal energy  $k_BT$ . If the position-dependent free energies of the system along coordinate x is given by F(x), the barrier crossing rate k from one energy minimum to another is given by

$$k = \frac{\sqrt{F''(x_{\min})|F''(x_{\max})|}}{2\pi\gamma} \exp \left(-\Delta F/k_{\rm B}T\right),\tag{2}$$

where  $x_{\min}$  and  $x_{\max}$  are the positions of the free energy minimum and barrier along the reaction coordinate,  $\Delta F \equiv$  $F(x_{\text{max}}) - F(x_{\text{min}})$  is the barrier height, and  $F'' \equiv d^2 F/dx^2$  is the curvature of the free energy landscape computed through second-order central finite differences.  $\gamma$  represents the friction constant, which was calculated as  $\gamma = 1.384 \times 3\pi \eta D$  according to the translational friction factor of cube-shaped particles.<sup>34</sup> The solvent viscosity  $\eta$  was assumed to be that of water at room temperature, i.e., 0.89 mPa s.

## Results and discussion

#### Assembly mechanism of bare nanocubes

As a first step to understanding the assembly pathway of surface-functionalized nanocubes, we studied the assembly behavior of bare nanocubes. The absence of ligand interactions makes this system a good control for dissecting the role of vdW interactions acting between the particle cores of surfacefunctionalized NPs in their assembly. The free energy landscape computed for bare nanocubes is depicted in Fig. 2a and it reveals that their free energy F is negligible across the vast majority of the configurational space compared to its value at the FF configuration ( $d_s = 0$ ,  $d_v = D$ ,  $\theta = 0^\circ$ ) representing the global minimum in the landscape. This is even more apparent in the 2D representations of the 3D landscape shown in Fig. 2b and c, where the portrayed energies represent F values

Nanoscale Paper

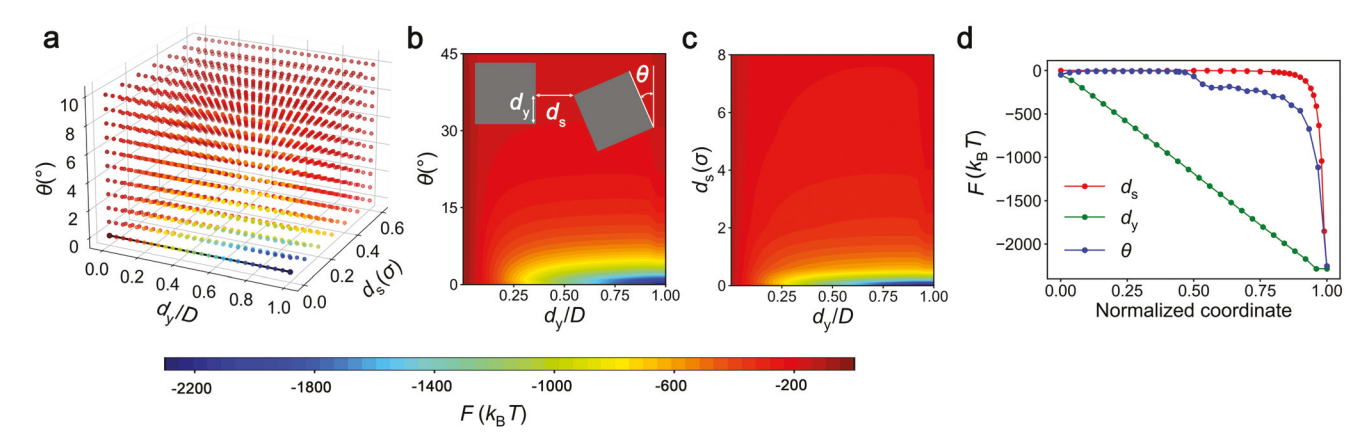


Fig. 2 Assembly of bare nanocubes with  $\varepsilon_{cc} = k_B T$ . (a) Free energy landscape  $F(d_s, d_v, \theta)$  showing the FF configuration as the global MFE state. The solid black line is the MFEP between the tip-to-tip and FF configurations depicted by solid black circles. (b) Free energy with respect to  $d_v$  and  $\theta$  for values of  $d_s$  that minimize F. (c) Free energy with respect to  $d_v$  and  $d_s$  for values of  $\theta$  that minimize F. (d) Free energy as nanocubes transition from the dissociated state to the ideal face-face state ( $d_s = 0$ ,  $d_v = D$ ,  $\theta = 0^\circ$ ) with purely a single type of association mechanism. Color bar at the bottom applies to (a)-(c).

at the indicated two coordinate values minimized with respect to the third coordinate; for instance, in Fig. 2b, we have plotted  $F(d_v, \theta)$  at values of  $d_s$  that yield the lowest free energy at those  $(d_v, \theta)$ . Both sets of results show that bare nanocubes assemble in the FF configuration and that their free energy decays sharply with deviations from this configuration.

To gain insight into the assembly mechanism of bare nanocubes, we analyzed the free energy pathway of bare nanocubes as they transition from a dissociated state to the FF state, first purely through a single association mechanism (Fig. 2d). Specifically, the change in F through a purely lineal association (LA) mechanism was examined by varying  $d_s$  from D to 0 while the other two coordinates were kept fixed at  $d_v = D$  and  $\theta = 0^\circ$ . The sliding association (SA) mechanism was probed by changing  $d_y$  from 0 to D with fixed  $d_s = 0$  and  $\theta = 0^\circ$ . Lastly, the rolling association (RA) mechanism was examined by changing  $\theta$  from 90° to 0° with  $d_s = 0$  and  $d_v = D$ . To make the comparison of the three mechanisms more convenient, the changes in the configuration of the nanocubes are normalized so that the fully dissociated state has a value of 0 and the FF state a value of 1 in the normalized coordinate system. The results demonstrate that the magnitude of F increases linearly with respect to  $d_{\nu}$  throughout the SA mechanism. However, for both the RA and LA mechanisms, F is negligible for most configurations except near the FF configuration where the free energies change drastically. In addition, the energetic penalty for deviating from the FF configuration is greater through lineal motion than through rolling motion. This is because lineal dissociation (LD) involves dissociation of atoms across the entire surface of the nanocubes while rolling dissociation (RD) leads to separation of only a fraction of the atoms, as the atoms on the edges of the nanocubes remain associated.

In the above analysis, both the SA and RA mechanisms start from the same tip-to-tip configuration of nanocubes, but follow distinct paths towards the same FF configuration—the global MFE state of bare nanocubes. While the free energy profiles plotted in Fig. 2d clearly suggest that SA would be the favored pathway over RA, it is unclear if SA also is the MFEP between these two configurations. We therefore determined the MFEP between the tip-to-tip and FF configurations in the free energy landscape and found that the SA indeed represents the MFEP between the two states (see Fig. 2a).

#### Assembly mechanism of surface-functionalized nanocubes

As observed in our previous study, 15 surface-functionalized nanocubes exhibit stable FF, EE, and I states, with the globally stable (global MFE) state switching between the three states depending on the strength  $\varepsilon_{\rm cc}$  of the vdW interactions between the nanocubes and the excluded volume  $\sigma_{
m lig}$  of the ligand segments (Fig. 3a). In particular, increasing  $\sigma_{\text{lig}}$  causes the nanocubes to transition from the FF to the I to the EE states, while increasing  $\varepsilon_{cc}$  causes the opposite sequence of transitions. We previously showed that these transitions occur because both the attractive vdW interactions between nanocubes and the repulsive steric interactions between ligands are the strongest for the FF state and the weakest for the EE state. This means that the FF state is energetically favored when the system is dominated by attractive interactions (large  $\varepsilon_{cc}$  and small  $\sigma_{lig}$ ) and the EE state is favored when repulsive interactions dominate (small  $\varepsilon_{cc}$  and large  $\sigma_{lig}$ ), while the I state is favored at intermediate conditions. Thus, to properly study the assembly pathway of surface-functionalized nanocubes, we examined nanocube systems with different vdW interaction strengths and ligand segment excluded volumes, as indicated by rectangles in Fig. 3a, which gave us access to all three varieties of nanocubes, i.e., FF-, I-, and EE-forming nanocubes. For MFEP analyses, we again chose the tip-to-tip configuration ( $d_s = 0$ ,  $d_v$ = 0,  $\theta$  = 0°) to be the initial state, as this was the configuration with the most favorable free energy among all the dissociated configurations shown in Fig. 2d. We then determined the MFEP from the tip-to-tip configuration to the local energy

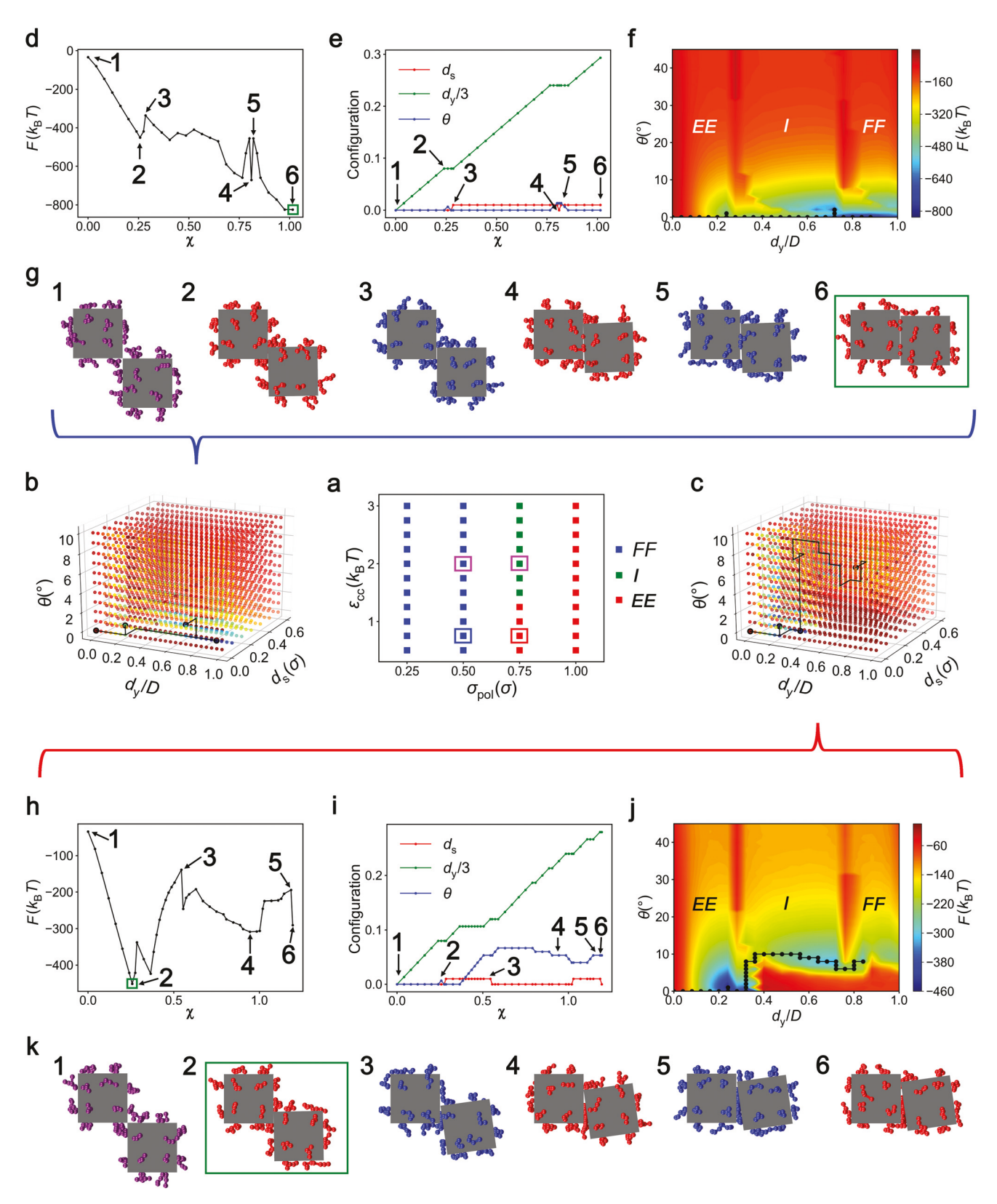


Fig. 3 Assembly pathway of surface-functionalized nanocubes with weak vdW interactions. (a) Phase diagram with respect to  $\sigma_{\text{lig}}$  and  $\varepsilon_{\text{cc}}$ . (b-k) Results corresponding to  $[\sigma_{\text{lig}}, \varepsilon_{\text{cc}}] = [0.5\sigma, 0.75k_{\text{B}}T]$  (b, d-g) and  $[0.75\sigma, 0.75k_{\text{B}}T]$  (c, h-k). (b and c) Free energy landscapes  $F(d_s, d_y, \theta)$  showing the MFEPs as black lines and the local or global MFE configurations as solid black circles. (d and h) Free energy along the MFEP. (e and i) Nanocube configuration coordinates along the MFEP. (f and j) Free energy with respect to  $d_v$  and  $\theta$  minimized with respect to  $d_s$ . (g and k) Representative nanocube configurations at specific points along the MFEP indicated in (d and h) and (e and i). Configurations at the tip-to-tip, metastable/stable, and transition states are distinguished by purple, red, and blue grafts. Green rectangle denotes the globally stable state. Color bars in (f) and (j) also apply to (b) and (c), respectively.

Nanoscale

b C a d 40 0.3 Configuration 1.0 7.0  $d_{\rm v}/3$ -800 -1000  $F(k_{\rm B}T)$ 30 -1200 F 6 6 20 -1600 -2000 -2000 10 -2400 -2800 -3000 0.0 0.00 0.25 0.50 0.75 0.00 0.25 0.50 0.75 1.00 0.2 0.6  $d_{v}/D$ d f е g -100 40 -250 -300 Configuration 1.0  $d_{\rm v}/3$ 30 -500 -500 F ⊕ 6 20 -700 -750 -900 -1000 10 7 -1300 0.0 1.0 0.5 0.6 0.8 0.5 1.0 0.2 1.0  $d_{\nu}/D$ 

Fig. 4 Assembly pathway of surface-functionalized nanocubes with strong vdW interactions. (a–h) Results corresponding to  $[\sigma_{iig}, \varepsilon_{cc}] = [0.5\sigma, 2k_BT]$  (a–d) and  $[0.75\sigma, 2k_BT]$  (e–h). (a and e) Free energy along the MFEP. (b and f) Nanocube configuration coordinates along the MFEP. (c and g) Free energy with respect to  $d_y$  and  $\theta$  minimized with respect to  $d_s$ . (d and h) Representative nanocube configurations at specific points along the MFEP indicated in (a and e) and (b and f). Configurations at the tip-to-tip, metastable/stable, and transition states are distinguished by purple, red, and blue grafts. Green rectangle denotes the globally stable state.

minimum state in the *EE* phase, then MFEP from *EE* to *I*, and finally the MFEP from *I* to *FF*.

We first examined nanocubes with weak vdW interactions  $(\varepsilon_{\rm cc}=0.75\varepsilon)$  that formed the FF phase when  $\sigma_{\rm lig}=0.5\sigma$  (blue rectangle in Fig. 3a) and the EE phase when  $\sigma_{\rm lig}=0.75\sigma$  (red rectangle). The free energy landscapes and MFEPs computed for these two systems are depicted in Fig. 3b and c. Compared to bare nanocubes (Fig. 2a), surface-functionalized nanocubes exhibit weaker attraction and more complex variations in free energy with respect to configuration, especially for nanocubes grafted with ligands of larger segments (Fig. 2c). Fig. 3d–f plot the progression of free energy and configuration of the nanocubes along the MFEP of the FF-forming nanocubes, where  $d_y/D < 0.25$  indicates the EE phase,  $d_y/D \geq 0.75D$  signifies the FF phase, and  $0.25 \leq d_y/D < 0.75D$  corresponds to the I phase. Similar to the assembly of bare nanocubes, the association

mechanism involves mainly SA (Fig. 3e). As the nanocubes slide toward the FF configuration, the free energy varies almost linearly with respect to  $d_v$ . However, unlike bare nanocubes, the MFEP here harbors several energy barriers as the nanocubes transition from the EE to the I to the FF phase (Fig. 3d). To help understand the origin of these barriers, we inspected nanocube configurations at the energy barriers (transition states) and wells (metastable states), as shown in Fig. 3g. We can observe that the metastable states labelled 2 and 4 correspond to configurations in which the surfaces of the nanocubes attempt to maximize their interaction area  $(\propto d_v)$  in the EE and I phases without crossing over to the next phase. On the other hand, the transition states labelled 3 and 5 occur as the surfaces of the nanocubes dissociate from each other to incorporate more grafts. While such dissociation incurs large energy penalty, it is a necessary step for the nanocubes to transition

Paper

configuration.

from one phase to another. The results plotted in Fig. 3e indicate that the dissociation at the first transition state follows a largely LD mechanism. This is followed by a prolonged SA concluded by a small RA leading to the *I* phase with a face–edge contact. At the second transition state, the dissociation occurs *via* a combination of LD and RD, which brings the nanocube surfaces to a parallel configuration. This is then followed by another prolonged SA to the *FF* phase, the global MFE

The MFEP of the EE-forming nanocubes displays many similarities with that of the FF-forming nanocubes described above. In particular, the free energy along the MFEP (Fig. 3h) displays multiple energy wells and barriers, and the assembly mechanism is again dominated by SA interspersed with combinations of LD, RA, and RD motions (Fig. 3i and k). However, the nanocubes are less parallel and involve larger rolling motions compared to the FF-forming nanocubes (Fig. 3e). For example, the EE-forming nanocubes are parallel only in the EE state (labelled 2 in Fig. 3h-k) and remain in slanted configurations with face-edge contacts ( $\theta > 0^{\circ}$  and  $d_s = 0$ ) in contrast to the parallel, surface-separated ( $\theta = 0^{\circ}$  and  $d_{\rm s} > 0$ ) configurations observed for the FF-forming nanocubes in Fig. 3d. This distinction in the assembly mechanism arises because the rolling motion affects the edge atoms and the rest of the atoms of the nanocubes differently depending on  $\sigma_{lig}$ . As  $d_s$  is large when  $\sigma_{
m lig}$  is large, the gain in vdW interaction energy by atoms on the edge of the nanocube as the nanocubes transition from parallel to the slanted configuration is larger than the loss in vdW energy by the rest of the atoms on the interacting surfaces of the nanocubes. However, for FF-forming nanocubes where  $\sigma_{\text{lig}}$  is small, the vdW energy gained by the edge atoms is smaller and the energy loss by the rest of the surface atoms is larger. Thus, the degree of involvement of rolling and lineal mechanisms in the dissociation of the nanocubes depends on the strength of repulsive interactions mediated by the grafted ligands.

In addition to weakly interacting nanocubes, we also investigated the FF-forming ( $\sigma_{\text{lig}} = 0.5\sigma$ ) and I-forming ( $\sigma_{\text{lig}} = 0.75\sigma$ ) nanocubes with strong vdW interactions ( $\varepsilon_{cc} = 2\varepsilon$ ) marked by purple rectangles in Fig. 3a. The shape of the free energy profile along the MFEP as well as the assembly mechanism of the FF-forming nanocubes with strong interactions shown in Fig. 4a-d are very similar to those with weak interactions depicted in Fig. 3d-g, except for two notable differences. First, the magnitude of free energies are obviously much larger in nanocubes with strong interactions. Second, no energy barrier exists between the I and FF states. This is because the vdW interactions are now even more dominant and the increased free volume available to the grafts from the rolling motion does not outweigh the reduction in vdW energy. Consequently, the nanocubes prefer to remain parallel throughout the transition from the *I* to the *FF* state.

Lastly, the *I*-forming nanocubes with strong vdW interactions also assemble similarly to *EE*-forming nanocubes with weak interactions, except that the MFE state now is the *I* rather than the *EE* phase. This is clearly a result of the stronger vdW

interactions being able to overcome the steric repulsion from the grafts enclosed between the nanocube surfaces in the *I* phase. Since vdW interactions dominate steric repulsion in these *I*-forming nanocubes, the free energy is also consistently larger in magnitude across the MFEP.

While we have compared the strongly and weakly interacting nanocubes by modifying  $\varepsilon_{cc}$ , the above results also provide insight into the effect of nanocube size on their assembly behavior. Experimentally, Klinkova et al. have shown that polystyrene-grafted silver nanocubes tend to form homogeneous FF structures when the particles are large (D = 45 nm) whereas they form less uniform configurations consisting mostly of I and EE configurations for smaller D (25 nm).3 Our previous calculations<sup>15,35</sup> have shown the interaction free energy between nanocubes scales more sharply with size for the FF state  $(\propto D^2)$  compared to the I state  $(\propto D)$ . Therefore, the larger the nanocube, the greater its preference for the FF configuration. In addition, because the interaction strengths are weaker for smaller nanocubes, the height of free-energy barriers between metastable states will also be reduced, resulting in less uniform configurations for smaller nanocubes.

#### Effect of surface roughness

While the MFEPs presented in Fig. 3 and 4 provide useful insights into the assembly mechanism of surface-functionalized nanocubes, the predicted energy barriers between metastable states are  $O(100k_BT)$ . As most assembly experiments, such as those involving Ag nanocubes, 1,2 are conducted at temperatures of 270-400 K and over time scales of hours, the large barriers imply that the nanocubes would not be able to transition between different stable phases within observable time scales. While this result could well be valid for many experimental cases in which thermal annealing does not alter the assembly configuration of nanocubes, it cannot explain the thermally-induced transition from EE to FF phases observed by Gao et al. One possible cause of this discrepancy could be the overestimation of the vdW interaction energy between nanocubes due to our assumption of "ideal" nanocubes. In particular, our model assumes that the nanocubes are defectless, so their surfaces are atomically smooth. However, atomic force microscope imaging of Ag nanocubes revealed that their surface is not perfectly flat but has a root mean squared deviation of one to two atomic diameters. 16 Such surface roughness can lead to a drastic reduction in the vdW interactions energy between faceted NPs as only a fraction of the surface atoms can be in contact with the other NP. Indeed, computational studies have shown that NPs transition from an associated percolating gel to a dissociated fluid phase when surface roughness is incorporated.36

To investigate the effects of roughness, we also obtained the MFEP of atomically corrugated "rough" nanocubes as introduced earlier. Fig. 5 presents the results obtained for such nanocubes with parameters ( $\sigma_{\rm lig} = 0.5\sigma$ ,  $\varepsilon_{\rm cc} = 0.75\varepsilon$ ) and ( $\sigma_{\rm lig} = 0.5\sigma$ ,  $\varepsilon_{\rm cc} = 2\varepsilon$ ), which lead to the *FF* phase in case of ideal nanocubes (see Fig. 3a). Similar to the MFEP of ideal nanocubes, the *FF* phase is the global MFE state for rough nano-

Nanoscale Paper

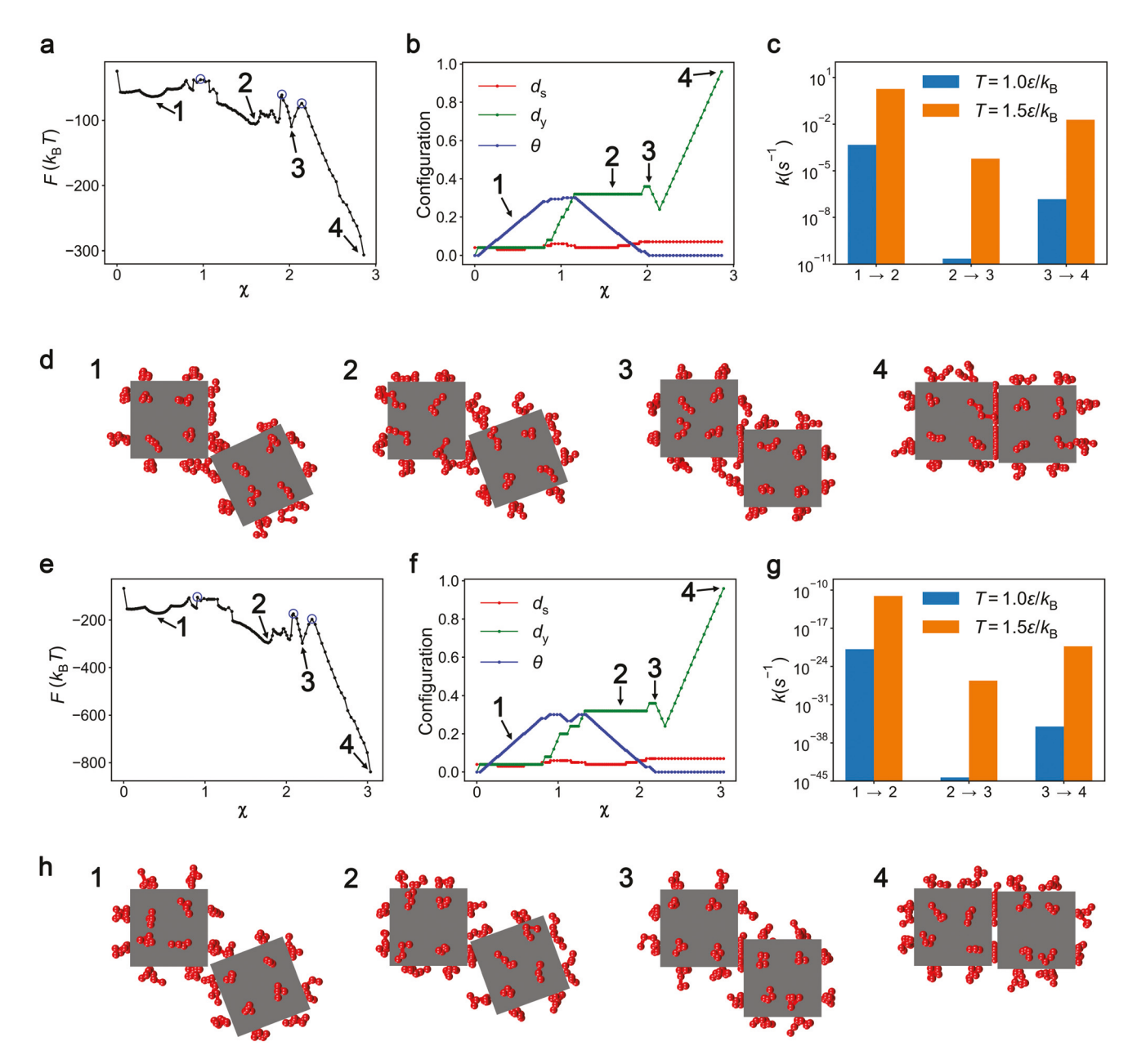


Fig. 5 Assembly pathway and transition rates of nanocubes with rough surfaces. (a–h) Results corresponding to  $[\sigma_{lig}, \varepsilon_{cc}] = [0.5\sigma, 0.75k_BT]$  (a–d) and [0.5σ, 2k<sub>B</sub>T] (e-h). (a and e) Free energy along the MFEP. Transition states between energy minima are marked by blue circles. (b and f) Nanocube configuration coordinates along the MFEP. (c and g) Transition rates between energy minima at the two specified temperatures. (d and h) Representative nanocube configurations at specific points along the MFEP indicated in (a and e) and (b and f).

cubes. The mechanism of assembly from the I phase (labelled 3 in Fig. 5d and h) to the FF phase (labelled 4) also is dominated mostly by the SA mechanism. Furthermore, as was the case with ideal nanocubes, the assembly mechanism is very similar between rough nanocubes with large and small  $\varepsilon_{\rm cc}$ .

However, two key differences emerge between the MFEPs of rough and ideal nanocubes. First, the overall magnitude of the free energy of rough nanocubes is ≈30% of that of ideal nanocubes. Consequentially, the energy barriers between different states are also significantly smaller. For example, for the MFEP

obtained with parameters of ( $\sigma_{\text{lig}} = 0.5\sigma$ ,  $\varepsilon_{\text{cc}} = 0.75\varepsilon$ ), the energy barrier between the *EE* and the *I* phase is  $\approx 25k_BT$  (Fig. 5a) while it is  $\approx 115k_{\rm B}T$  for ideal nanocubes (Fig. 3d). Second, the assembly mechanism of rough nanocubes involves much more lineal and rolling motions. This is because the energy loss of the nanocubes from LD and RD is greatly reduced as less number of atoms are in contact with each other due to surface roughness.

A consequence of reduced interaction energies between nanocubes is that the kinetics of many of the transitions across phases are now within experimental time scales. In fact,

using Kramer's theory we can estimate the rate of transition from the *EE* to the *I* phase (labelled  $1 \rightarrow 2$  in Fig. 5c) for rough nanocubes with  $\varepsilon_{cc} = 0.75\varepsilon$  at  $T = 1\varepsilon/k_B$  to be  $O(10^{-4} \text{ s}^{-1})$ , indicating that this transition now occurs within experimental time scales. On the other hand, the rate of the  $I \rightarrow FF$  transition (labelled  $3 \rightarrow 4$ ) is  $O(10^{-7} \text{ s}^{-1})$ , indicating that the probability of this transition occurring within experimental time scales is still very low. However, these results change drastically when thermal annealing is applied, for instance, when T is increased to  $1.5\varepsilon/k_{\rm B}$ , which is equivalent to changing the temperature from 270 K to 400 K in experiments. Now, the transition rates between all three phases are larger than  $O(10^{-5}$ s<sup>-1</sup>). Therefore, the nanocubes are expected to spontaneously assemble into their global MFE configuration, the FF phase, within experimental time scales. In contrast, the transition rate for rough nanocubes with  $\varepsilon_{\rm cc} = 2\varepsilon$  are all less than  $O(10^{-10}$ s<sup>-1</sup>), indicating that a large fraction of these nanocubes are likely to be observed trapped in one or more of its metastable states (Fig. 5g). From these results, one can infer that the thermally-induced  $EE \rightarrow FF$  transition experimentally observed by Gao et al. likely belongs to the case where the energy barriers are such that thermal annealing is necessary for the transition to take place in experimental time scales, similar to the computational results shown in Fig. 5c.

## Conclusions

We have computationally investigated the assembly mechanism of surface-functionalized nanocubes by carrying out MFEP analyses of their interaction free energy landscape. Our results show that the nanocubes exhibit multiple metastable states related to the FF, I, and EE phases reported earlier, and that the MFEP connecting these metastable states contains transition states with large free energy barriers. Analysis of nanocube configurations along the MFEP revealed that the transition between metastable states requires slight dissociation of the nanocubes, which allows them to incorporate more grafted ligands between their interacting faces. In general, the dissociation mechanism involves lineal separation of the nanocubes, while their ensuing progressive association towards the next metastable state follows a combination of sliding and rolling motions. In the future, it would be important to experimentally test these assembly pathway predictions using new, powerful spectroscopy techniques such as multimodal single-molecule FRET337 and fluorescence correlation spectroscopy,<sup>38</sup> which can measure spatiotemporal changes in the relative location of fluorescent molecules strategically tagged onto the system of interest.

We also demonstrated that, similar to the globally stable state, the assembly pathway too is determined by the competition between attractive vdW interactions and repulsive steric interactions mediated by the nanocube cores and grafts, respectively. Specifically, increasing the strength of vdW interactions leads to more parallel configurations of the nanocubes and reduced rolling motions throughout the MFEP, whereas

increasing the magnitude of steric interactions leads to more slanted configurations and pronounced rolling motions. Incorporation of surface roughness to the nanocubes greatly reduces the overall magnitude of vdW interactions between the nanocubes. Apart from making the lineal and rolling motions of the assembly pathway more pronounced, roughness leads to significant lowering of energy barriers that can cause some prohibitively slow transitions across metastable states to become more kinetically accessible. In some cases, thermal annealing is required to make transitions between metastable and stable states more kinetically accessible.

On the whole, this work suggests that the design of surfacefunctionalized NPs to target a specific assembly configuration needs to consider not only the globally stable state but also the MFEP leading to this state. For example, while our previous study<sup>15</sup> suggested that strong attractive interactions between the nanocube cores will always lead to the FF state being favored, the results of this study indicate that the transition towards the FF state from the I or EE configurations might not occur within experimental time scales if the linear and rolling dissociative motions required between states incur large energetic penalties. Therefore, the interaction strength between the NPs needs to be adjusted so that the activation energy between metastable states is relatively weak while the energy well at the targeted configuration is much deeper compared to those of the metastable states. Such insights not only help explain the heterogeneity in interparticle configurations and thermallyinduced transitions between them observed experimentally, 1-3 but they should also help engineer experimental systems that lead to more uniform assembly of nanocubes into targeted nanostructures.

## Conflicts of interest

There are no conflicts to declare.

## Acknowledgements

We thank Prof. Andrea Tao for valuable discussions. This work was sponsored in part by the National Science Foundation (Grant No. CMMI 1636356) and by the UC San Diego Materials Research Science and Engineering Center (UCSD MRSEC) supported by the National Science Foundation (Grant No. DMR-2011924). Computational resources were provided by the Duke Computing Cluster (DCC) and the Extreme Science and Engineering Discovery Environment (XSEDE) Program supported by the National Science Foundation (Grant No. ACI-1053575).

## References

1 B. Gao, G. Arya and A. R. Tao, Self-orienting nanocubes for assembly of plasmonic nanojunctions, Nanotechnol., 2012, 7, 433-437.

Nanoscale

2 K. L. Gurunatha, S. Marvi, G. Arya and A. R. Tao, Computationally Guided Assembly of Oriented Nanocubes by Modulating Grafted Polymer–Surface Interactions, *Nano Lett.*, 2015, 15, 7377–7382.

- 3 A. Klinkova, H. Thérien-Aubin, A. Ahmed, D. Nykypanchuk, R. M. Choueiri, B. Gagnon, A. Muntyanu, O. Gang, G. C. Walker and E. Kumacheva, Structural and optical properties of self-assembled chains of plasmonic nanocubes, *Nano Lett.*, 2014, 14, 6314–6321.
- 4 F. Lu, T. Vo, Y. Zhang, A. Frenkel, K. G. Yager, S. Kumar and O. Gang, Unusual packing of soft-shelled nanocubes, *Sci. Adv.*, 2019, 5, eaaw2399.
- 5 Z. Quan, H. Xu, C. Wang, X. Wen, Y. Wang, J. Zhu, R. Li, C. J. Sheehan, Z. Wang, D.-M. Smilgies, *et al.*, Solvent-mediated self-assembly of nanocube superlattices, *J. Am. Chem. Soc.*, 2014, 136, 1352–1359.
- 6 M. N. O'Brien, M. Girard, H.-X. Lin, J. A. Millan, M. O. De La Cruz, B. Lee and C. A. Mirkin, Exploring the zone of anisotropy and broken symmetries in DNA-mediated nanoparticle crystallization, *Proc. Natl. Acad. Sci. U. S. A.*, 2016, 113, 10485–10490.
- 7 K. C. Elbert, W. Zygmunt, T. Vo, C. M. Vara, D. J. Rosen, N. M. Krook, S. C. Glotzer and C. B. Murray, Anisotropic nanocrystal shape and ligand design for co-assembly, *Sci. Adv.*, 2021, 7, eabf9402.
- 8 S.-W. Hsu, A. L. Rodarte, M. Som, G. Arya and A. R. Tao, Colloidal plasmonic nanocomposites: from fabrication to optical function, *Chem. Rev.*, 2018, **118**, 3100–3120.
- 9 B. D. Clark, C. R. Jacobson, M. Lou, D. Renard, G. Wu, L. Bursi, A. S. Ali, D. F. Swearer, A.-L. Tsai, P. Nordlander, *et al.*, Aluminum nanocubes have sharp corners, *ACS Nano*, 2019, **13**, 9682–9691.
- 10 R. Das and S. Sarkar, Optical properties of silver nanocubes, *Opt. Mater.*, 2015, **48**, 203–208.
- 11 B. Gao, Y. Alvi, D. Rosen, M. Lav and A. R. Tao, Designer nanojunctions: orienting shaped nanoparticles within polymer thin-film nanocomposites, *Chem. Commun.*, 2013, **49**, 4382–4384.
- 12 N. Hooshmand, H. S. Mousavi, S. R. Panikkanvalappil, A. Adibi and M. A. El-Sayed, High-sensitivity molecular sensing using plasmonic nanocube chains in classical and quantum coupling regimes, *Nano Today*, 2017, 17, 14– 22.
- 13 Y. H. Lee, W. Shi, Y. Yang, Y.-C. Kao, H. K. Lee, R. Chu, Y. L. Pang, C. L. Lay, S. Li and X. Y. Ling, Modulating Orientational Order to Organize Polyhedral Nanoparticles into Plastic Crystals and Uniform Metacrystals, *Angew. Chem.*, 2020, 132, 21369–21375.
- 14 C. Knorowski and A. Travesset, Self-Assembly and Crystallization of Hairy (f-Star) and DNA-Grafted Nanocubes, *J. Am. Chem. Soc.*, 2014, **136**, 653–659.
- 15 B. H.-j. Lee and G. Arya, Orientational phase behavior of polymer-grafted nanocubes, *Nanoscale*, 2019, **11**, 15939–15957.
- 16 X. Xia, M. Rycenga, D. Qin and Y. Xia, A silver nanocube on a gold microplate as a well-defined and highly active sub-

- strate for SERS detection, *J. Mater. Chem. C*, 2013, **1**, 6145-6150
- 17 M. Sun, L. Xu, J. H. Bahng, H. Kuang, S. Alben, N. A. Kotov and C. Xu, Intracellular localization of nanoparticle dimers by chirality reversal, *Nat. Commun.*, 2017, 8, 1–10.
- 18 B. H.-j. Lee, N. A. Kotov and G. Arya, Reconfigurable Chirality of DNA-Bridged Nanorod Dimers, *ACS Nano*, 2021, **15**, 13547–13558.
- 19 J. S. Rowlinson and F. L. Swinton, *Liquids and liquid mixtures*, Butterworth-Heinemann, 1982.
- 20 J. I. Siepmann and D. Frenkel, Configurational bias Monte Carlo: a new sampling scheme for flexible chains, *Mol. Phys.*, 1992, 75, 59–70.
- 21 P. L. M. de Maupertuis, *Memoirs of the Royal Academy of Sciences of Paris*, Institut de France, 1744, pp. 417–426.
- 22 G. Henkelman, B. P. Uberuaga and H. Jónsson, A climbing image nudged elastic band method for finding saddle points and minimum energy paths, *J. Chem. Phys.*, 2000, 113, 9901–9904.
- 23 S. A. Trygubenko and D. J. Wales, A doubly nudged elastic band method for finding transition states, *J. Chem. Phys.*, 2004, **120**, 2082–2094.
- 24 E. Weinan, W. Ren and E. Vanden-Eijnden, String method for the study of rare events, *Phys. Rev. B: Condens. Matter Mater. Phys.*, 2002, 66, 052301.
- 25 R. W. Floyd, Algorithm 97: shortest path, *Commun. ACM*, 1962, 5, 345.
- 26 P. E. Hart, N. J. Nilsson and B. Raphael, A formal basis for the heuristic determination of minimum cost paths, *IEEE Trans. Syst. Man Cybern. Syst.*, 1968, 4, 100–107.
- 27 B. V. Cherkassky, A. V. Goldberg and T. Radzik, Shortest paths algorithms: Theory and experimental evaluation, *Math. Program.*, 1996, 73, 129–174.
- 28 I. Marcos-Alcalde, J. Setoain, J. I. Mendieta-Moreno, J. Mendieta and P. Gómez-Puertas, MEPSA: minimum energy pathway analysis for energy landscapes, *Bioinformatics*, 2015, **31**, 3853–3855.
- 29 E. Seitz and J. Frank, POLARIS: path of least action analysis on energy landscapes, *J. Chem. Inf. Model.*, 2020, 60, 2581– 2590.
- 30 E. W. Dijkstra, A note on two problems in connexion with graphs, *Numer. Math.*, 1959, 1, 269–271.
- 31 J. Kirk, Dijkstra's Shortest Path Algorithm, https://www.mathworks.com/matlabcentral/fileexchange/12850-dijkstras-shortest-path-algorithm, 2021.
- 32 H. A. Kramers, Brownian motion in a field of force and the diffusion model of chemical reactions, *Physica*, 1940, 7, 284–304.
- 33 G. Arya, Models for recovering the energy landscape of conformational transitions from single-molecule pulling experiments, *Mol. Simul.*, 2016, 42, 1102–1115.
- 34 K. Okada and A. Satoh, Evaluation of the translational and rotational diffusion coefficients of a cubic particle (for the

- application to Brownian dynamics simulations), *Mol. Phys.*, 2020, **118**, e1631498.
- 35 B. H.-j. Lee and G. Arya, Analytical van der Waals interaction potential for faceted nanoparticles, *Nanoscale Horiz.*, 2020, 5, 1628–1642.
- 36 J. D. Olarte-Plata, G. Brekke-Svaland and F. Bresme, The influence of surface roughness on the adhesive interactions and phase behavior of suspensions of calcite nanoparticles, *Nanoscale*, 2020, **12**, 11165–11173.
- 37 S. Kilic, S. Felekyan, O. Doroshenko, I. Boichenko, M. Dimura, H. Vardanyan, L. C. Bryan, G. Arya, C. A. Seidel and B. Fierz, Single-molecule FRET reveals multiscale chromatin dynamics modulated by HP1α, *Nat. Commun.*, 2018, 9, 1–14.
- 38 J.-J. Song, R. Bhattacharya, H. Kim, J. Chang, T.-Y. Tang, H. Guo, S. K. Ghosh, Y. Yang, Z. Jiang, H. Kim, *et al.*, One-dimensional anomalous diffusion of gold nanoparticles in a polymer melt, *Phys. Rev. Lett.*, 2019, **122**, 107802.